NANO LETTERS

Letter

pubs.acs.org/NanoLett

Two-Dimensional SiS Layers with Promising Electronic and Optoelectronic Properties: Theoretical Prediction

Ji-Hui Yang,*[,†,∥] Yueyu Zhang,[‡,§] Wan-Jian Yin,[†] X. G. Gong,[‡,§] Boris I. Yakobson,[∥] and Su-Huai Wei*[,⊥]

[†]National Renewable Energy Laboratory, Golden, Colorado 80401, United States

[‡]Key Laboratory for Computational Physical Sciences (MOE), State Key Laboratory of Surface Physics, Department of Physics, Fudan University, Shanghai 200433, China

[§]Collaborative Innovation Center of Advanced Microstructures, Nanjing 210093, China

[∥]Department of Materials Science and NanoEngineering, Rice University, Houston, Texas 77005, United States

[⊥]Beijing Computational Science Research Center, Beijing 100094, China

Supporting Information

ABSTRACT: Two-dimensional (2D) semiconductors can be very useful for novel electronic and optoelectronic applications because of their good material properties. However, all current 2D materials have shortcomings that limit their performance. As a result, new 2D materials are highly desirable. Using atomic transmutation and differential evolution global optimization methods, we identified two group IV−VI 2D materials, *Pma*2-SiS and silicene sulfide. *Pma*2-SiS is found to be both chemically, energetically, and thermally stable. Most importantly, *Pma*2-SiS has shown good electronic and optoelectronic properties, including direct bandgaps suitable for solar cells, good mobility for nanoelectronics, good flexibility of property tuning by layer control and applied strain, and good air stability as well. Therefore, *Pma*2-SiS is expected to be a promising 2D material in the field of 2D electronics and optoelectronics. The designing principles demonstrated in identifying these two tantalizing examples have great potential to accelerate the finding of new functional 2D materials.

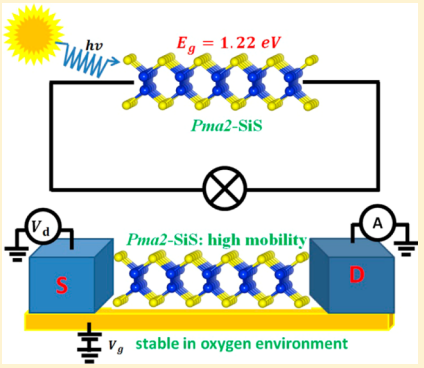

KEYWORDS: *SiS, direct bandgap, high mobility, stability, differential evolution, global structure search*

Two-dimensional (2D) materials have recently attracted great interest due to novel properties suitable for electronic and optoelectronic applications. Current studies are mainly focused on graphene,[1−4] transition metal dichalcogenides (TMDs),[5−9] and phosphorene,[10−12] to design novel nanoelectronic devices such as field effect transistors and solar cells. Blue phosphorus is also proposed with interesting properties.[13] Although these 2D materials have demonstrated many promising electronic and optoelectronic properties compared to 3D materials, their disadvantages are also becoming more apparent, limiting their applications. For example, graphene, as the first extensively studied 2D material, has excellent carrier mobility,[14,15] but its semimetallic behavior and lack of bandgap limit its applications in electronics. Monolayer TMDs such as MoS_2, show direct bandgaps[5] and self-healing properties in air,[16] but their less dispersive band edges with relatively localized transition metal d character[17] result in relatively heavy carrier effective masses[18,19] and thus not so good mobility for high-performance applications.[20,21] Moreover, bandgaps turn from being direct into indirect when TMDs change from mono- to multilayers,[5] thus limiting the flexibility of tuning its electronic properties through layer controls. Phosphorene and few-layer black phosphorus have shown good mobility[10] and good flexibility of tuning properties by layer control and anisotropic engineering.[22,23] However, their poor stability leads to rapid degradation when exposed to air.[24,25] While much effort has been devoted to improving the properties of these 2D materials, it also shows great necessity and urgency to find and design new 2D materials.

One of the approaches in the new materials design is "atomic transmutation" in which one type of elements is changed (transmutated) into its neighboring elements in the periodic table but the total number of valence electrons is kept unchanged. Great success has been achieved in 3D materials. For example, ZnSe has a band gap of 2.8 eV, which is too large for solar cell application. By transmutating two Zn atoms in ZnSe into one Cu and one Ga, $CuGaSe_2$ is obtained with a bandgap of 1.7 eV. Further mutating two Ga atoms in $CuGaSe_2$ into one Zn and one Sn leads to $Cu_2ZnSnSe_4$ with a bandgap of 1.0 eV.[26,27] Both $CuGaSe_2$ and $Cu_2ZnSnSe_4$ have shown great promises for photovoltaic applications. Similarly, by transmutating two Si atoms in silicon into one Al and one P, Si_3AlP is recently obtained with much better light absorption than Si.[28] In 2D materials, it is well-known that by transmutating two C

Received: October 26, 2015
Revised: December 23, 2015
Published: January 7, 2016

DOI: 10.1021/acs.nanolett.5b04341
Nano Lett. 2016, 16, 1110−1117

atoms in group IV graphene into one B atom and one N atom, monolayer group III−V material h-BN can be obtained with wide bandgap and new functionalities.[29] For example, it can serve as an ideal substrate for two-dimensional electronics,[30,31] a tunneling material for vertical tunneling devices, and a growth template for heterostructures.[32] Recently, Zhu et al.[33] applied this well-known idea to group V elemental 2D material phosphorene by replacing two P atoms in phosphorene or in monolayer blue phosphorus by one Si atom and one S atom and predicted new 2D materials α-SiS and β-SiS with interesting properties. In their study, they followed previous conventions of atomic transmutation by keeping the parent lattices unchanged and omitting a global structure search. However, in 2D materials this type of practice is not justified. For example, α-SiS and β-SiS in ref 33 are expected to be unstable due to their three coordinated Si and S bonds. More advanced material design methods based on atomic transmutation should go beyond the conventional practice by exploring the global structure stability. This is important for the realization of new materials, especially in 2D systems. Motivated by this reasoning, here we design new 2D SiS structures using global search based on the differential evolution (DE) method. In fact, as we see below many structures are found that are energetically more stable than the previously proposed α-SiS and β-SiS; among them two new structures stand out with very attractive properties. The first one, *Pma*2-SiS, has the lowest total energy among all the structures studied here and is 0.74 eV/f.u. lower than the α-SiS and β-SiS structures in previous study[33] and is predicted to have high mobility, direct bandgap, good optical absorption, good tunability of its electronic properties through layer control, anisotropy, or applied strain, and good stability in air as well. The other one is the metastable "silicene sulfide", which has a total energy of 0.69 eV/f.u. lower than α-SiS and β-SiS and has similar properties as the *Pma*2-SiS. We expect that our findings can stimulate new interests in the field of 2D optoelectronic and electronic applications.

We have performed DE search many times with different $(SiS)_n$ ($n \leq 6$) cells and the final stable structures are selected by comparing their total energies. The lowest energy structure of Si_2S_2 obtained from our search is shown in Figure 1a with top and side views. Because it has *Pmma* symmetry, we name it as *Pmma*-SiS. The optimized lattice parameters are a = 3.326 Å and b = 3.994 Å with these two lattice vectors orthogonal to each other. In *Pmma*-SiS, Si atoms form zigzag chains along b directions (see bc-plane projections in Figure 1a), which are sandwiched and also connected by two S layers. Each Si atom is bonded to two other Si atoms and two S atoms while each S atom is bonded to two Si atoms. As a result, the system obeys the "octet rule", which means that both S and Si atoms have eight valence electrons to fully occupy the outmost sp shells and each bond (including S dangling bonds) contains two electrons, thus this structure should be chemically stable. However, our calculated phonon spectrum for this Si_2S_2 cell shows that there is one small imaginary frequency around X point (see Supporting Information), which implies that periodicity of atomic arrangements along a direction should be doubled. Indeed, we found by DE search that eight-atom "supercell" Si_4S_4, which doubles the lattice vector along a direction and has lattice parameters of a = 6.644 Å and b = 3.985 Å, is dynamically more stable. As can be seen from bc-plane projection in Figure 1c, both top and bottom S atom layers are alternatively slightly rotated around the a-axis or

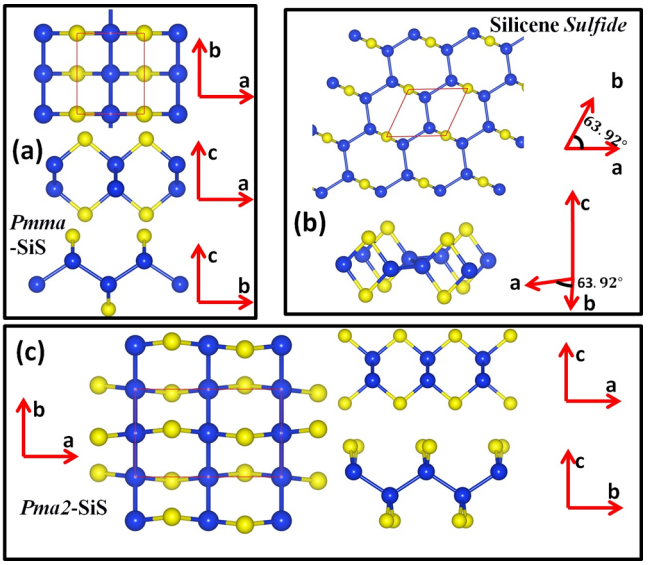

Figure 1. Top and side views of structures for (a) *Pmma*-SiS, (b) silicene sulfide of *Cmmm* symmetry, and (c) *Pma*2-SiS. Blue is for Si and yellow is for S atoms.

titled toward positive and negative b direction. This long-range periodicity in S layers lowers the total energy slightly and removes the imaginary frequency from the phonon spectrum (see Supporting Information). Consequently, the structure in Figure 1c is both chemically and dynamically stable. Because this structure has *Pma*2 symmetry, we name it as *Pma*2-SiS. Both *Pmma*-SiS and *Pma*2-SiS have direct bandgaps at Γ point. In the following, we mainly discuss the electronic properties of *Pma*2-SiS and consider the electronic properties of *Pmma*-SiS only when we discuss the band foldings from *Pmma*-SiS to *Pma*2-SiS (see the band structure of *Pmma*-SiS in Supporting Information). The formation energy ΔH_f(*Pma*2-SiS) of *Pma*2-SiS, defined as the total energy difference E(*Pma*2-SiS) − E(Si) − E(S), is −0.85 eV/f.u., indicating that *Pma*2-SiS is energetically stable against decomposition into bulk Si and S. Note that, compared to α-SiS and β-SiS proposed in ref 33, which have formation energies of −0.09 and −0.11 eV/f.u., the *Pma*2-SiS structure is much more stable. We also tried DE search in yet larger 12-atom cells but we did not find new structures that are more stable than *Pma*2-SiS.

Besides *Pmma*-SiS and *Pma*2-SiS, we also found another interesting structure in Si_2S_2 unit cell, as shown in Figure 1b. In this structure, all the Si atoms are in ab-plane and form stretched honeycomb lattices with top and bottom S layers inserted into Si−Si bonds. The optimized lattice parameters are a = 4.563 Å, b = 4.011 Å, and the angle between the lattice vectors is 63.92°. Because of the similarity between this structure and unbuckled silicene and graphene oxide,[34,35] we name it as silicene sulfide, which has *Cmmm* symmetry. In this structure, both Si and S atoms also obey "octet rule" and thus it should be chemically stable. The formation energy of silicene sulfide is −0.80 eV/f.u., indicating that it is energetically stable. Similar to *Pma*2-SiS, in silicene sulfide Si atoms also form zigzag chains, which are now lying in the ab-plane, whereas in *Pma*2-SiS the zigzag chains are standing in the ab-plane. Because of their structural similarity, their total energies only differ by 50 meV/f.u.. Phonon calculations of silicene sulfide show no imaginary frequency, indicating that it is dynamically stable (see Supporting Information).

DOI: 10.1021/acs.nanolett.5b04341
Nano Lett. 2016, 16, 1110−1117

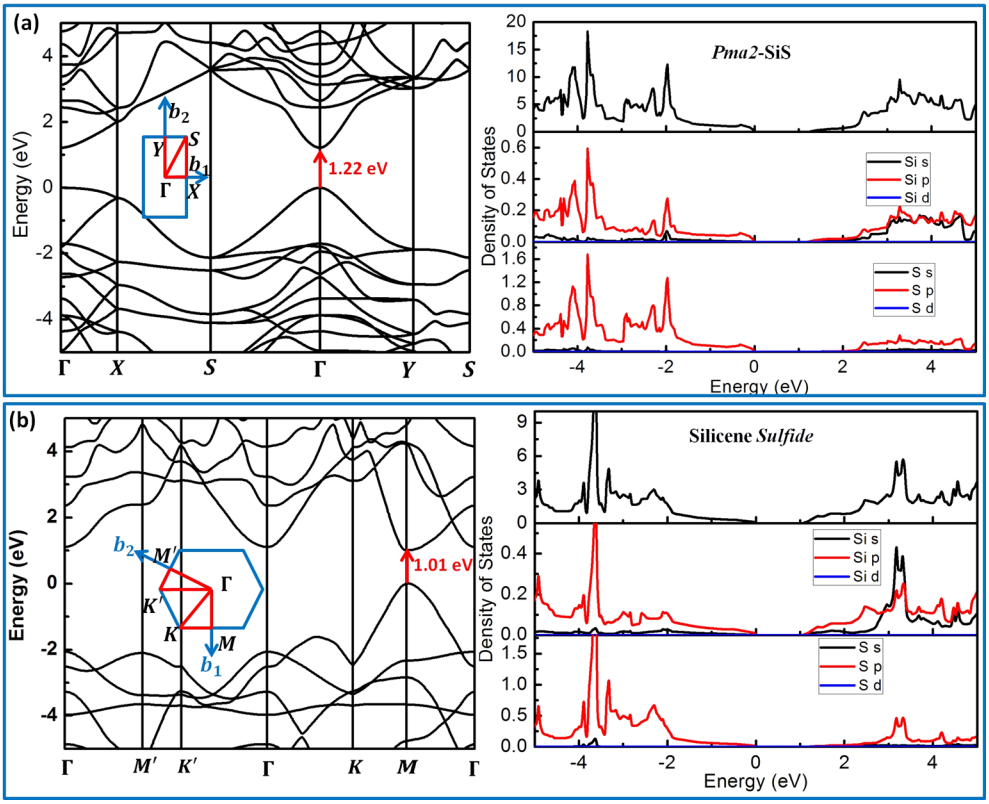

Figure 2. Band structures and (partial) density of states for (a) *Pma*2-SiS and (b) silicene sulfide.

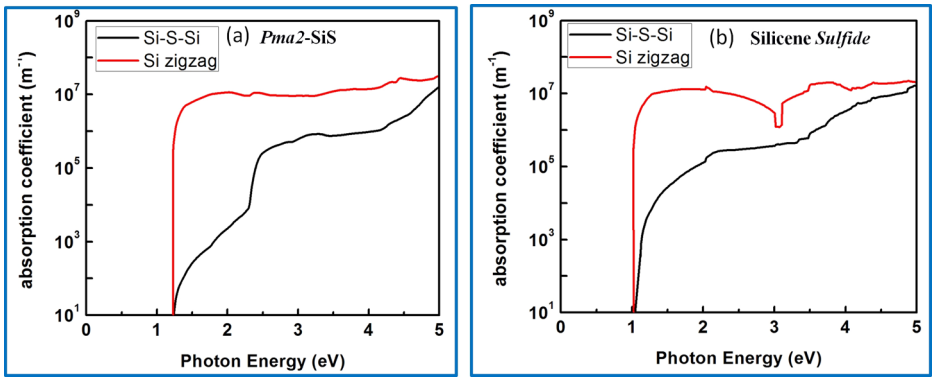

Figure 3. Calculated optical absorption coefficients for (a) *Pma*2-SiS and (b) silicene sulfide for polarization along Si−S−Si bond directions and along Si zigzag chain directions.

We also checked the thermal stabilities of these structures and found that *Pma*2-SiS can still stay stable at T = 300 K but silicene sulfide becomes slightly buckled, which is somewhat expected because silicene has the buckling tendency at the room temperature (see Supporting Information). Both *Pma*2-SiS and silicene sulfide can still keep their structures even at T = 500 K.

The band structures and density of states of *Pma*2-SiS and silicene sulfide are shown in Figure 2. Clearly, both of them are direct bandgap semiconductors with bandgaps of 1.22 and 1.01 eV for *Pma*2-SiS and silicene sulfide, respectively, from the HSE06 calculations. It is well-known that HSE06 calculations in general cannot give accurate and physical bandgap values in 2D systems due to neglect of excitons. However, considering that in 2D systems the underestimation of HSE06 bandgaps compared to the quasi-particle *GW* bandgaps can somewhat cancel the effect of neglecting excitons,[36,37] the HSE06 optical bandgap values are close to the real optical bandgap. For example, our HSE06 bandgap of phosphorene is 1.6 eV, which is in good agreement with the experimental result of 1.45 eV.[12] We also performed G_0W_0 calculations for our structures and then obtained the optical bandgaps using the scaling law in ref 36. Our results for the optical bandgaps of *Pma*2-SiS and silicene sulfide are 1.35 and 1.14 eV, respectively (see Supporting Information). The optical bandgap values are close to HSE06 calculations and thereby we mainly use HSE06 results during the following discussions. Their partial density of states indicates that the valence band maximum (VBM) mainly consists of Si p state and S p state while the conduction band minimum (CBM) contains Si s and p states and S p state, which is also confirmed by the site projected wave function characters. As a result, the optical transitions between band-

DOI: 10.1021/acs.nanolett.5b04341
Nano Lett. 2016, 16, 1110−1117

Table 1. Calculated Carrier Effective Masses, Deformation Potentials, Elastic Moduli, and Carrier Mobilities along Si Zigzag Chain Direction (Denoted as x) and Si−S−Si Bond Direction (Denoted as y) in *Pma2*-SiS and Silicene Sulfide at T = 300 K

structure		$\frac{m_x^*}{m_0}$	$\frac{m_y^*}{m_0}$	E_{1x} (eV)	E_{1y} (eV)	C_x (jm^{-2})	C_y (jm^{-2})	μ_x (cm^2 V^{-1} s^{-1})	μ_y (cm^2 V^{-1} s^{-1})
Pma2-SiS	electron	0.16	0.50	4.77	1.33	67.60	111.50	1.40×10^3	9.49×10^3
	hole	0.24	5.92	3.71	1.52	67.60	111.50	3.66×10^2	1.46×10^2
silicene sulfide	electron	0.12	1.06	9.49	1.57	54.31	56.71	3.00×10^2	1.30×10^3
	hole	0.19	0.52	3.59	0.64	54.31	56.71	1.50×10^3	1.80×10^4

edges are allowed. As seen in Figure 3, both *Pma*2-SiS and silicene sulfide show good optical absorptions at their direct bandgaps. Because their optical bandgaps are close to the optimal values required for solar cell absorbers, they can be good candidate semiconductors for photovoltaic applications. What's more, both of them show strong optical anisotropies. The light absorptions along Si zigzag chains are much stronger than that along the directions of the Si−S−Si bonds. The strong optical anisotropies can be understood by that the optical transition is dominant by transitions between Si p and s states, which is stronger along Si zigzag chains. Due to this property, both *Pma*2-SiS and silicene sulfide could be good candidates for polarized optical sensors.

Besides the good optical properties, *Pma*2-SiS and silicene sulfide also show very promising electrical transport properties. Table 1 shows their calculated carrier effective masses, which are generally smaller than effective masses in TMDs and comparable to the effective masses in phosphorene,[38] mainly due to the more dispersive p and s characters of VBM and CBM. In addition, both electrons and holes show relatively small effective masses along the direction of Si zigzag chains compared to those along Si−S−Si bond directions. As a result, anisotropic electronic transport behaviors are expected.

To further explore their transport properties for potential electronic applications, we need to know the carrier mobility in *Pma*2-SiS and silicene sulfide. To estimate their mobility, we used the following expression[23,39,40]

$$\mu = \frac{e\hbar^3 C}{k_B T m_e^* m_d (E_1^i)^2} \quad (1)$$

where m_e^* is the carrier effective mass along the transport direction and m_d is the carrier average effective mass determined by $m_d = \sqrt{m_x^* m_y^*}$. Here x and y represent Si zigzag direction and Si−S−Si bond direction, orthogonal to each other. The term E_1^i represents the deformation potential constant of the VBM for hole or CBM for electron along the transport direction, defined by $E_1^i = \Delta V_i/(\Delta l/l_0)$, where ΔV_i is the energy change of VBM or CBM when the system is compressed or dilated from the equilibrium distance l_0 by a distance of Δl along the transport direction. The term C is the elastic modulus of the longitudinal strain in the propagation directions (both x and y) of the longitudinal acoustic wave, which is derived from $(E - E_0)/S_0 = C(\Delta l/l_0)^2/2$, where E is the total energy and S_0 is the equilibrium lattice area. Here we used $\Delta l/l_0$ from −0.2% to 0.2% to fit the values for C and E_1^i (see Supporting Information) and the obtained carrier mobility is listed in Table 1. As we can see, both *Pma*2-SiS and silicene sulfide show strong electrical transport bias; the electron mobility is higher than hole mobility in *Pma*2-SiS while hole mobility is higher in silicene sulfide. Besides, the carrier mobility difference is much larger along Si−S−Si bond direction than along Si zigzag chain direction. More importantly, the carrier mobility in both *Pma*2-SiS and silicene sulfide is large, which are comparable or even larger than that in phosphorene[40] at room temperature (2300 cm^2 V^{-1} s^{-1}). For example, electron mobility along Si−S−Si bond direction in *Pma*2-SiS can reach 9.5×10^3 cm^2 V^{-1} s^{-1} and hole mobility along Si−S−Si bond direction in silicene sulfide can be as large as 1.8×10^4 cm^2 V^{-1} s^{-1} at T = 300 K. The high carrier mobility mainly results from two aspects. First, the elastic modulus C is large, which is expected from the hybridized covalent sp^3 bonds, which are strong and difficult to be compressed or dilated. Second, the band edge deformation potentials are generally small along Si−S−Si bond directions. This can be further understood by considering the band edge wave functions. As shown in Figure 4, in *Pma*2-SiS the VBM electron states mainly distribute along Si zigzag chain direction. As a result, the lattice deformation along Si−S−Si bond direction has less effect on the VBM positions. For the CBM, electron states mainly locate on Si atoms, which have less overlap along Si−S−Si bond direction than Si zigzag chain direction, mainly due to the larger distance between Si atoms along Si−S−Si bond direction. Consequently, the lattice deformation along Si−S−Si bond direction also has less effect on the CBM positions. Same arguments can explain the small CBM deformation potential in silicene sulfide. For the VBM in silicene sulfide, because the electron states distribute in parallel with Si zigzag chain direction and have little overlap along the Si−S−Si bond direction, the VBM deformation potential along Si−S−Si bond direction is the smallest in our study. Together with the relatively small carrier effective mass and moderately large elastic modulus along this direction, a very high hole mobility is attained.

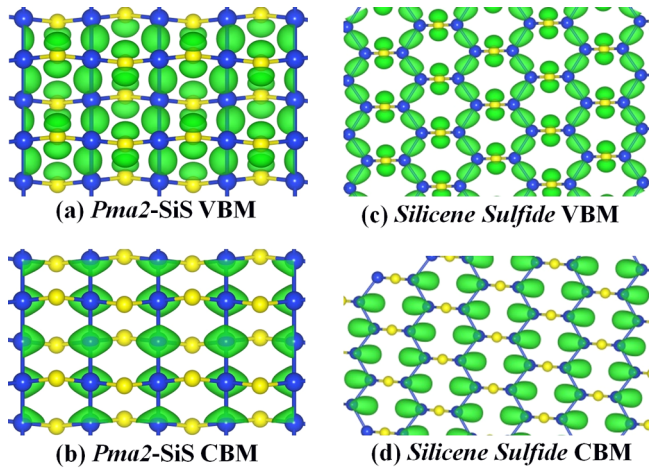

Figure 4. Partial charge density shown in green for (a) the VBM and (b) the CBM of *Pma*2-SiS; (c) the VBM and (d) the CBM of silicene sulfide.

DOI: 10.1021/acs.nanolett.5b04341
Nano Lett. 2016, 16, 1110−1117

Because eq 1 just considers the coupling between free carriers and acoustic phonons, it can overestimate the carrier mobility considering that in reality, carriers can also be scattered by other factors such as defects. To further confirm our estimations of carrier mobility, we also adopted an alternative method, in which the mobility can be obtained by $\mu = \sigma/en$, where σ is the carrier conductivity, n is the carrier density, and e is the elementary charge. Both σ and n are functions of electron potentials or Fermi levels. While σ can be obtained using classical Boltzmann transport theory with the approximation of a constant carrier relaxation time,[41] n can be easily calculated from density of states at given electron potentials.[41] Detailed equations about this method are provided in the Supporting Information. We compared the calculated mobility in phosphorene and in our SiS systems by assuming a common carrier relaxation time, which is fitted as around 250 fs to match the experimentally measured mobility in phosphorene (1000 $cm^2 V^{-1} s^{-1}$).[10] As clearly shown in Figure 5, the carrier mobility in *Pma*2-SiS and silicene sulfide along Si zigzag chain direction is about 2−3 times higher than the carrier mobility in phosphorene along its armchair direction. Although these two methods of estimating carrier mobility have differences due to the use of different approximations, the general results are consistent that both *Pma*2-SiS and silicene sulfide could have high carrier mobility comparable or even larger than phosphorene. As a result, they are expected to be suitable for nanoelectronic applications such as FETs.

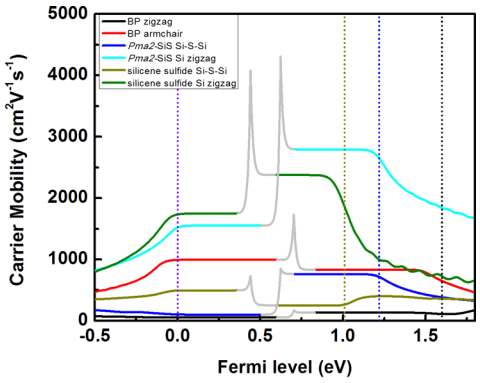

Figure 5. Comparisons of carrier mobility in monolayer black phosphorus, *Pma*2-SiS, and silicene sulfide. The VBMs are set as zero Fermi levels for these three systems, as indicated by the vertical dashed violet line. The CBMs of monolayer black phosphorus, *Pma*2-SiS, and silicene sulfide are indicated by vertical dashed black, blue, and dark yellow lines, respectively. Note that the peaks near the middle of bandgaps caused by the too small and inaccurate carrier densities ($\mu = \sigma/en$) are not accurate and reliable and indicated by light gray lines. The plateaus above the VBMs stand for the hole mobility while the plateaus below the CBMs stand for the electron mobility.

As 2D materials, the electronic properties of *Pma*2-SiS and silicene sulfide are expected to be tunable by controlling layer numbers and/or by applying strain, which has been widely used in both 2D[12,42,43] and 3D systems.[44−49] For example, two layers of *Pma*2-SiS with AA-stacking show a reduced but still direct bandgap of 1.03 eV while two layers of silicene sulfide with AA-stacking gives a direct bandgap of 0.99 eV (see Supporting Information). When strain is applied to monolayer *Pma*2-SiS and silicene sulfide, their electronic bandgaps can also be tuned. As seen in Figure 6, by applying a small 2% biaxial compressive strain, the bandgap of *Pma*2-SiS increases from 1.22 to 1.58 eV, which is still direct and closer to the optimal value for photovoltaic absorbers. When 6% strain is applied, the bandgap can be as large as 2.40 eV. Besides, when the biaxial compressive strain is larger than 4%, *Pma*2-SiS shows a direct to indirect bandgap transition with CBM moving from the Γ point to *X* point (see Supporting Information). This transition is mainly induced by *a*-direction compressive strains and is similar to what is observed in bulk zinc-blend semiconductor with tetrahedral bonds.[50] On the other hand, under the tensile strains *Pma*2-SiS keeps its direct bandgaps independent of the directions of the applied strain. Generally speaking, bandgaps increase with the compressive strains and decrease with tensile strains in *Pma*2-SiS. Things are different in silicene sulfide. The bandgaps are more sensitive to uniaxial strains than to biaxial strains. The latter always tend to decrease bandgaps of silicene sulfide while keeping them direct at the *M* point. This interesting behavior is caused by the opposite effects of *a*-direction strains and *b*-direction strains. While *b*-direction strains keep the direct bandgap increasing with the compressive strains, *a*-direction strains make the direct bandgaps decrease. The opposite trends also happen when tensile strains are applied. As a result, direct to indirect bandgap transitions occur only when single axial strains are applied with CBM moving from *M* point to Γ point (see Supporting Information).

Finally, we will discuss the defect properties in *Pma*2-SiS and its stability in ambient environment. Similar to MoS_2, in *Pma*2-SiS, the surfaces are also covered by S atoms. When S vacancies are formed during the growth or postgrowth operations of

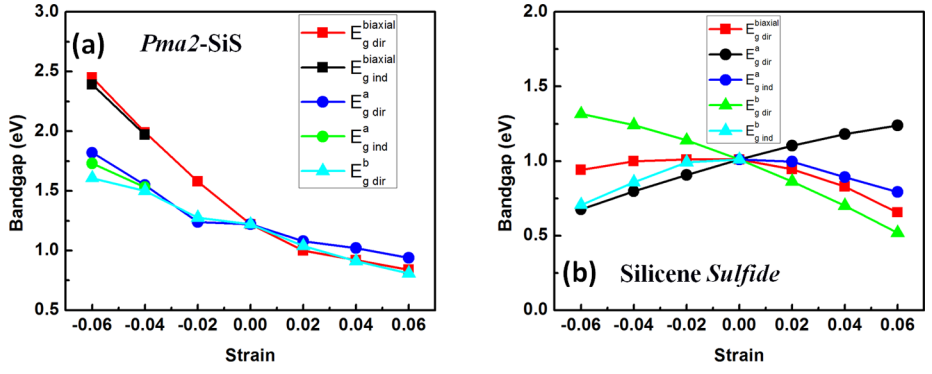

Figure 6. Bandgaps dependence on biaxial and uniaxial strains in (a) *Pma*2-SiS and (b) silicene sulfide. In the subscripts of the labels, "dir" means "direct" and "ind" means "indirect". The superscripts stand for the directions of the strains.

DOI: 10.1021/acs.nanolett.5b04341
Nano Lett. 2016, 16, 1110−1117

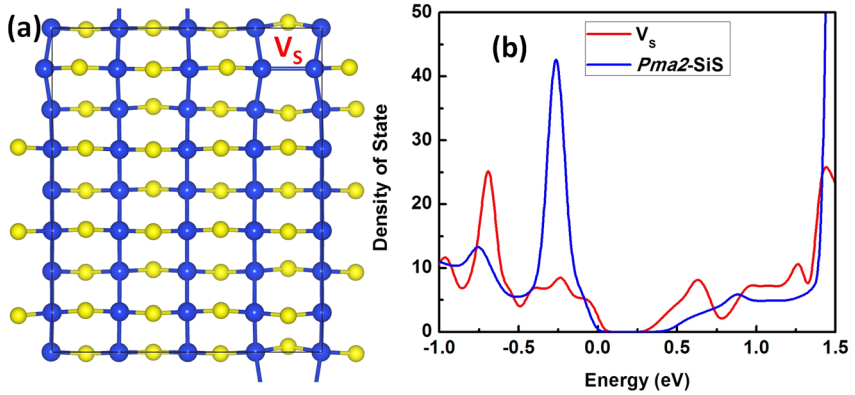

Figure 7. (a) Atomic configuration of sulfur vacancy in *Pma2*-SiS. (b) Density of states in *Pma2*-SiS supercells with and without sulfur vacancy.

MoS_2, deep gap states are created, which can act as carrier traps and charge scattering centers, reducing the carrier mobility. However, things are different in *Pma2*-SiS because the defects are much more benign, mainly due to self-healing of the Si bonds. When a S vacancy is created on the surface of *Pma2*-SiS, the two Si atoms near this vacancy will spontaneously get close to each other and are reconstructed to form a Si−Si bond, as shown in Figure 7a. In this case, all the atoms in the system still obey "octet rule" and no gap states are created (see Figure 7b). When exposed to the air, oxygen is considered to be the main factor causing instabilities of 2D materials, especially for phosphorene, which shows rapid degradation in an hour after exfoliation.[24] However, in TMDs it has been shown that oxygen is not so harmful and instead, oxygen can passivate chalcogen vacancies and thus improve device performances.[16] Similar things are expected in *Pma*2-SiS because S and O are isovalent, except that *Pma*2-SiS does not even need passivation. To further confirm the air stability, we also considered oxygen defects in *Pma*2-SiS, including O on S site and O interstitials, as shown in Supporting Information Figure S13. Again, none of these defects create gap states because the "octet rule" still holds. As a result, *Pma*2-SiS is expected to have good air stability, at least not inferior to TMDs.

In summary, using atomic transmutation and a global differential evolution (DE) search scheme, we have identified new 2D group IV−VI materials, including *Pma*2-SiS and silicene sulfide, which are expected to have good material properties for various optoelectronic and electronic applications. They have direct bandgap with high light absorption suitable for photovoltaic applications, high mobility for nanoelectronics, strong optical and electronic anisotropies for optical sensors, and good ambient environment stability. These combined properties indicate that they are very promising candidates for 2D optoelectronic and electronic applications. Although the focus of this work is on theoretical predictions, experimental confirmations are strongly called for, and silicene might be a good starting point to synthesize these 2D SiS semiconductors at low temperatures, as we noticed that graphene oxide with 1:1 O:C ratio is already synthesized.[35]

Methods. *DE-Based Global Optimization Method for 2D Material Design.* We use differential evolution method to design 2D materials as implemented in the IM2ODE package.[51,52] Differential evolution is a global optimization algorithm to search the multidimensional continuous spaces to best fit to the target functions.[53] In the basic DE algorithm, each solution candidate is treated as a vector in the *D*-dimensional space and involves three steps: mutation, crossover, and selection. The mutation operation generates a mutant vector $\mathbf{v}$ for the ith target vector $\mathbf{x}$ in the population as follows

$$\mathbf{v}_{i,G+1} = \gamma \mathbf{x}_{\text{best},G} + (1-\gamma)\mathbf{x}_{i,G} + F(\mathbf{x}_{r1,G} - \mathbf{x}_{r2,G}) \quad (2)$$

where G denotes the generation, $\mathbf{x}_{\text{best},G}$ denotes the best solution of the Gth generation, $r1$ and $r2$ are random indexes in the population that are mutually different from i, parameter γ represents the "greediness" of the operator, and F is a parameter that controls the effect of differential vector. Crossover step creates the trial vector $\mathbf{u}_{i,G+1} = (u_{1i,G+1}, u_{2i,G+1},...,u_{Di,G+1})$ according to the following scheme:

$$\mathbf{u}_{ji,G+1} = \begin{cases} \mathbf{v}_{ji,G+1}, & \text{if} \quad r(j) \le CR \quad \text{or} \quad j = rn(i) \\ \mathbf{x}_{ji,G}, & \text{if} \quad r(j) > CR \quad \text{and} \quad j \ne rn(i) \end{cases} \quad (3)$$

where $r(j) \in [0,1]$ is the jth uniformly generated random number, $rn(i)$ represents a randomly chosen index of dimension to ensure the ith target vector gets at least one element from the mutant vector, and $CR \in [0,1]$ is the crossover probability. Selection in DE simply takes the greedy principle, that is, accepting the trial vector only if it is better than the previous corresponding target vector. Three important parameters γ, F, and CR in DE control the general behaviors of the algorithms and in this work we choose $\gamma = 0.1$, $F = 0.2$, and $CR = 1.0$. By the above operations, new solutions are created from one generation to the next. In structure search problems, the solutions are basically atom coordinates and the target functions are total energies.[54,55] When generating the initial structures or new structures during the global optimization process, the use of symmetry constrain[56−58] can often significantly improve the efficiency, therefore, we adopted this constrain when we need to generate new random structures in each DE step. After all structures are generated either by DE operations or by new random generations in each step, each of the structures is relaxed to the local minimum using first-principles calculations. In our study, we used 20 generations or 20 DE steps. For each DE step, 60% structures are inherited from last step by DE operations while 40% structures are newly added from random generations with symmetry constrain to avoid being trapped into local minimum.

First-Principles Calculation Methods. Our first-principles calculations were performed using density functional theory (DFT)[59,60] as implemented in the VASP code.[61,62] The electron and core interactions are included using the frozen-core projected augmented wave approach.[63] For all the

DOI: 10.1021/acs.nanolett.5b04341
Nano Lett. 2016, 16, 1110−1117

structure relaxations, we used generalized gradient approximation formulated by PBE.[64] For systems with more than one layer, van der Waals interactions are considered using zero damping DFT-D3 method of Grimme et al.[65] The structures are relaxed until the atomic forces are less than 0.01 eV/Å and total energies are converged to 10^{-6} eV with the cutoff energy for plane-wave basis functions set to 400 eV. The phonon spectra are calculated using PHONONPY code.[66] For the other electronic calculations, we used Heyd−Scuseria−Ernzerhof (HSE06) hybrid functional[67] with default parameters to correct bandgap errors. The band structures are plotted using Wannier90 code[68] and the electrical conductivity is calculated using semiclassical Boltzmann transport theories based on constant relaxation time approximation as implemented in the BoltzWann code.[41] The electron mobility then can be obtained from the calculated electrical conductivity and carrier concentrations.

■ ASSOCIATED CONTENT

Supporting Information

The Supporting Information is available free of charge on the ACS Publications website at DOI: 10.1021/acs.nanolett.5b04341.

Atomic coordinates and phonon spectra of *Pmma*-SiS, *Pma*2-SiS, and silicene sulfide, molecular dynamical simulation results for *Pma*2-SiS and silicene sulfide at T = 300 and 500 K, quasiparticle G_0W_0 calculations of bandgaps for *Pma*2-SiS and silicene sulfide, band structures of *Pmma*-SiS, two layer *Pma*2-SiS and two layer silicene sulfide, deformation potential constants and elastic modulus fitting for *Pma*2-SiS and silicene sulfide along Si zigzag chain direction and Si−S−Si bond direction, calculation methods of mobility from electrical conductivity, band structure changes with biaxial and single axial strains for *Pma*2-SiS and silicene sulfide, atomic configurations and density of states of O interstitials and O substituting S in *Pma*2-SiS. (PDF)

■ AUTHOR INFORMATION

Corresponding Authors

*E-mail: Ji-Hui.Yang@nrel.gov, yangjh2010@gmail.com.
*E-mail: suhuaiwei@csrc.ac.cn.

Notes

The authors declare no competing financial interest.

■ ACKNOWLEDGMENTS

The work at NREL is funded by the U.S Department of Energy (DOE) under Contract No. DE-AC36-08GO28308 and the Laboratory Directed Research and Development Program under Grant No. 065K1601. The calculations are done on NREL peregrine supercomputer and on the National Energy Research Scientific Computing Center, which is supported by the Office of Science of the U.S. Department of Energy under Contract No. DE-AC02-05CH11231. Effort at Rice was supported by the U.S. Army Research Office MURI Grant W911NF-11-1-0362.

■ REFERENCES

(1) Geim, A. K.; Novoselov, K. S. *Nat. Mater.* **2007**, *6*, 183−191.
(2) Novoselov, K. S.; Geim, A. K.; Morozov, S. V.; Jiang, D.; Katsnelson, M. I.; Grigorieva, I. V.; Dubonos, S. V.; Firsov, A. A. *Nature* **2005**, *438*, 197−200.
(3) Novoselov, K. S.; McCann, E.; Morozov, S. V.; Fal'ko, V. I.; Katsnelson, M. I.; Zeitler, U.; Jiang, D.; Schedin, F.; Geim, A. K. *Nat. Phys.* **2006**, *2*, 177−180.
(4) Zhang, Y.; Tan, Y.-W.; Stormer, H. L.; Kim, P. *Nature* **2005**, *438*, 201−204.
(5) Mak, K. F.; Lee, C.; Hone, J.; Shan, J.; Heinz, T. F. *Phys. Rev. Lett.* **2010**, *105*, 136805.
(6) Splendiani, A.; Sun, L.; Zhang, Y.; Li, T.; Kim, J.; Chim, C.-Y.; Gall, G.; Wang, F. *Nano Lett.* **2010**, *10*, 1271−1275.
(7) Banerjee, S.; Richardson, W.; Coleman, J.; Chatterjee, A. *IEEE Electron Device Lett.* **1987**, *8*, 347−349.
(8) Radisavljevic, B.; Radenovic, A.; Brivio, J.; Giacometti, V.; Kis, A. *Nat. Nanotechnol.* **2011**, *6*, 147−150.
(9) Radisavljevic, B.; Kis, A. *Nat. Mater.* **2013**, *12*, 815−820.
(10) Li, L.; Yu, Y.; Ye, G. J.; Ge, Q.; Ou, X.; Wu, H.; Feng, D.; Chen, X. H.; Zhang, Y. *Nat. Nanotechnol.* **2014**, *9*, 372−377.
(11) Liu, H.; Du, Y.; Deng, Y.; Ye, P. D. *Chem. Soc. Rev.* **2015**, *44*, 2732−2743.
(12) Liu, H.; Neal, A. T.; Zhu, Z.; Luo, Z.; Xu, X.; Tománek, D.; Ye, P. D. *ACS Nano* **2014**, *8*, 4033−4041.
(13) Zhu, Z.; Tománek, D. *Phys. Rev. Lett.* **2014**, *112*, 176802.
(14) Das Sarma, S. D.; Adam, S.; Hwang, E. H.; Rossi, E. *Rev. Mod. Phys.* **2011**, *83*, 407.
(15) Bolotin, K. I.; Sikes, K. J.; Jiang, Z.; Klima, M.; Fudenberg, G.; Hone, J.; Kim, P.; Stormer, H. L. *Solid State Commun.* **2008**, *146*, 351−355.
(16) Lu, J.; Carvalho, A.; Chan, X. K.; Liu, H.; Liu, B.; Tok, E. S.; Loh, K. P.; Neto, A. H. C.; Sow, C. H. *Nano Lett.* **2015**, *15*, 3524−3532.
(17) Kang, J.; Tongay, S.; Zhou, J.; Li, J.; Wu, J. *Appl. Phys. Lett.* **2013**, *102*, 012111.
(18) Lebègue, S.; Eriksson, O. *Phys. Rev. B: Condens. Matter Mater. Phys.* **2009**, *79*, 115409.
(19) Yoon, Y.; Ganapathi, K.; Salahuddin, S. *Nano Lett.* **2011**, *11*, 3768−3773.
(20) Fuhrer, M. S.; Hone, J. *Nat. Nanotechnol.* **2013**, *8*, 146−147.
(21) Low, T.; Rodin, A. S.; Carvalho, A.; Jiang, Y.; Wang, H.; Xia, F.; Castro Neto, A. H. *Phys. Rev. B: Condens. Matter Mater. Phys.* **2014**, *90*, 075434.
(22) Xia, F.; Wang, H.; Jia, Y. *Nat. Commun.* **2014**, *5*, 4458.
(23) Qiao, J.; Kong, X.; Hu, Z.-X.; Yang, F.; Ji, W. *Nat. Commun.* **2014**, *5*, 4475.
(24) Koenig, S. P.; Doganov, R. A.; Schmidt, H.; Castro Neto, A. H.; Ozyilmaz, B. *Appl. Phys. Lett.* **2014**, *104*, 103106.
(25) Ziletti, A.; Carvalho, A.; Campbell, D. K.; Coker, D. F.; Castro Neto, A. H. *Phys. Rev. Lett.* **2015**, *114*, 046801.
(26) Chen, S.; Gong, X. G.; Walsh, A.; Wei, S.-H. *Appl. Phys. Lett.* **2009**, *94*, 041903.
(27) Chen, S.; Gong, X. G.; Walsh, A.; Wei, S.-H. *Phys. Rev. B: Condens. Matter Mater. Phys.* **2009**, *79*, 165211.
(28) Yang, J.-H.; Zhai, Y.; Liu, H.; Xiang, H.; Gong, X.; Wei, S.-H. *J. Am. Chem. Soc.* **2012**, *134*, 12653−12657.
(29) Kubota, Y.; Watanabe, K.; Tsuda, O.; Taniguchi, T. *Science* **2007**, *317*, 932−934.
(30) Dean, C. R.; Young, A. F.; Meric, I.; Lee, C.; Wang, L.; Sorgenfrei, S.; Watanabe, K.; Taniguchi, T.; Kim, P.; Shepard, K. L.; Hone, J. *Nat. Nanotechnol.* **2010**, *5*, 722−726.
(31) Lee, K. H.; Shin, H.-J.; Lee, J.; Lee, I.-Y.; Kim, G.-H.; Choi, J.-Y.; Kim, S.-W. *Nano Lett.* **2012**, *12*, 714−718.
(32) Park, J.-H.; Park, J. C.; Yun, S. J.; Kim, H.; Luong, D. H.; Kim, S. M.; Choi, S. H.; Yang, W.; Kong, J.; Kim, K. K.; Lee, Y. H. *ACS Nano* **2014**, *8*, 8520−8528.
(33) Zhu, Z.; Guan, J.; Liu, D.; Tománek, D. *ACS Nano* **2015**, *9*, 8284−8290.
(34) Huang, B.; Xiang, H.; Xu, Q.; Wei, S.-H. *Phys. Rev. Lett.* **2013**, *110*, 085501.
(35) Mattson, E. C.; Pu, H.; Cui, S.; Schofield, M. A.; Rhim, S.; Lu, G.; Nasse, M. J.; Ruoff, R. S.; Weinert, M.; Gajdardziska-Josifovska, M.; Chen, J.; Hirschmug, C. J. *ACS Nano* **2011**, *5*, 9710−9717.

DOI: 10.1021/acs.nanolett.5b04341
Nano Lett. 2016, 16, 1110−1117

(36) Choi, J.-H.; Cui, P.; Lan, H.; Zhang, Z. *Phys. Rev. Lett.* **2015**, *115*, 066403.
(37) Tran, V.; Soklaski, R.; Liang, Y.; Yang, L. *Phys. Rev. B: Condens. Matter Mater. Phys.* **2014**, *89*, 235319.
(38) Xiao, J.; Long, M.; Zhang, X.; Ouyang, J.; Xu, H.; Gao, Y. *Sci. Rep.* **2015**, *5*, 9961.
(39) Bruzzone, S.; Fiori, G. *Appl. Phys. Lett.* **2011**, *99*, 222108.
(40) Fei, R.; Faghaninia, A.; Soklaski, R.; Yan, J.-A.; Lo, C.; Yang, L. *Nano Lett.* **2014**, *14*, 6393−6399.
(41) Pizzi, G.; Volja, D.; Kozinsky, B.; Fornari, M.; Marzari, N. *Comput. Phys. Commun.* **2014**, *185*, 422−429.
(42) Fei, R.; Yang, L. *Nano Lett.* **2014**, *14*, 2884−2889.
(43) Shi, H.; Pan, H.; Zhang, Y.-W.; Yakobson, B. I. *Phys. Rev. B: Condens. Matter Mater. Phys.* **2013**, *87*, 155304.
(44) Jacobsen, R. S.; Andersen, K. N.; Borel, P. I.; Fage-Pedersen, J.; Frandsen, L. H.; Hansen, O.; Kristensen, M.; Lavrinenko, A. V.; Moulin, G.; Ou, H.; Peucheret, C.; Zsigri, B.; Bjarklev, A. *Nature* **2006**, *441*, 199−202.
(45) Zhu, J.; Liu, F.; Stringfellow, G. B.; Wei, S.-H. *Phys. Rev. Lett.* **2010**, *105*, 195503.
(46) Lai, K.; Nakamura, M.; Kundhikanjana, W.; Kawasaki, M.; Tokura, Y.; Kelly, M. A.; Shen, Z.-X. *Science* **2010**, *329*, 190.
(47) Yin, W.-J.; Chen, S.; Yang, J.-H.; Gong, X.-G.; Yan, Y.; Wei, S.-H. *Appl. Phys. Lett.* **2010**, *96*, 221901.
(48) Fischetti, M. V.; Ren, Z.; Solomon, P. M.; Yang, M.; Rim, K. *J. Appl. Phys.* **2003**, *94*, 1079.
(49) Haeni, J. H.; Irvin, P.; Chang, W.; Uecker, R.; Reiche, P.; Li, Y. L.; Choudhury, S.; Tian, W.; Hawley, M. E.; Craigo, B.; Tagantsev, A. K.; Pan, X. Q.; Streiffer, S. K.; Chen, L. Q.; Kirchoefer, S. W.; Levy, J.; Schlom, D. G. *Nature* **2004**, *430*, 758.
(50) Wei, S.-H.; Zunger, A. *Phys. Rev. B: Condens. Matter Mater. Phys.* **1999**, *60*, 5404.
(51) Zhang, Y.-Y.; Gao, W.; Chen, S.; Xiang, H.; Gong, X.-G. *Comput. Mater. Sci.* **2015**, *98*, 51.
(52) Chen, H.-Z.; Zhang, Y.-Y.; Gong, X.; Xiang, H. *J. Phys. Chem. C* **2014**, *118*, 2333.
(53) Storn, R.; Price, K. *J. Global Optimization* **1997**, *11*, 341−359.
(54) Chen, Z.; Jiang, X.; Li, J.; Li, S.; Wang, L. *J. Comput. Chem.* **2013**, *34*, 1046−1059.
(55) Li, Z.-L.; Li, Z.-M.; Cao, H.-Y.; Yang, J.-H.; Shu, Q.; Zhang, Y.-Y.; Xiang, H. J.; Gong, X. G. *Nanoscale* **2014**, *6*, 4309−4315.
(56) Wang, Y.; Lv, J.; Zhu, L.; Ma, Y. *Phys. Rev. B: Condens. Matter Mater. Phys.* **2010**, *82*, 094116.
(57) Wang, Y.; Lv, J.; Zhu, L.; Ma, Y. *Comput. Phys. Commun.* **2012**, *183*, 2063−2070.
(58) Pickard, C. J.; Needs, R. J. *J. Phys.: Condens. Matter* **2011**, *23*, 053201.
(59) Hohenberg, P.; Kohn, W. *Phys. Rev.* **1964**, *136*, B864−B871.
(60) Kohn, W.; Sham, L. J. *Phys. Rev.* **1965**, *140*, A1133−A1138.
(61) Kresse, G.; Furthmüller, J. *Phys. Rev. B: Condens. Matter Mater. Phys.* **1996**, *54*, 11169−11186.
(62) Kresse, G.; Furthmüller, J. *Comput. Mater. Sci.* **1996**, *6*, 15−50.
(63) Kresse, G.; Joubert, D. *Phys. Rev. B: Condens. Matter Mater. Phys.* **1999**, *59*, 1758−1775.
(64) Perdew, J. P.; Burke, K.; Ernzerhof, M. *Phys. Rev. Lett.* **1996**, *77*, 3865.
(65) Grimme, S.; Ehrlich, S.; Goerigk, L. *J. Comput. Chem.* **2011**, *32*, 1456−1465.
(66) Togo, A.; Tanaka, I. *Scr. Mater.* **2015**, *108*, 1−5.
(67) Heyd, J.; Scuseria, G. E.; Ernzerhof, M. *J. Chem. Phys.* **2003**, *118*, 8207.
(68) Mostofi, A. A.; Yates, J. R.; Lee, Y.-S.; Souza, I.; Vanderbilt, D.; Marzari, N. *Comput. Phys. Commun.* **2008**, *178*, 685−699.

DOI: 10.1021/acs.nanolett.5b04341
Nano Lett. 2016, 16, 1110−1117